The effect of interlayer on corrosion resistance of ceramic coating/Mg alloy substrate in simulated physiological environment

Guosong Wu [a], Ali Shanaghi [a], Ying Zhao [a], Xuming Zhang [a], Ruizhen Xu [a], Zhengwei Wu [a], Guangyao Li [b], Paul K. Chu [a,*]

[a] Department of Physics and Materials Science, City University of Hong Kong, Tat Chee Avenue, Kowloon, Hong Kong, China
[b] State Key Laboratory of Advanced Design and Manufacturing for Vehicle Body, Hunan University, Changsha 410082, China

ARTICLE INFO

ABSTRACT

Ceramic coatings are deposited on biodegradable magnesium alloys by physical vapor deposition to reduce the electrochemical activity in the simulated physiological environment. Although an interlayer is generally used to reduce the mismatch between the hard coating and soft substrate, the effects of the interlayer on the electrochemical corrosion behavior have seldom been explored. In this work, AlO_xN_y ceramic coatings were deposited on AZ31 magnesium alloys with Al or Ti interlayers. Polarization tests and electrochemical impedance spectroscopy (EIS) were conducted to evaluate the corrosion resistance in the cell culture medium. The AlO_xN_y ceramic coating significantly improved the bio-corrosion resistance of the magnesium alloy, but the Ti interlayer accelerated the corrosion rate. In comparison, although the addition of an Al interlayer led to smaller enhancement in the surface mechanical properties of the AlO_xN_y coating, corrosion could be impeded effectively. Our results indicate that an Al interlayer is preferred over Ti and the corrosion failure mechanism is discussed from the perspective of defects.

© 2012 Elsevier B.V. All rights reserved.

1. Introduction

Magnesium-based materials are attractive to the aerospace and automotive industry due to the low density and high specific strength. Recently, they have also been considered as revolutionary metallic biomaterials due to their favorable biodegradation and Young's modulus (about 40 GPa) similar to that of human bone [1–5]. In clinical practice, it is possible to skip a second surgery to remove the implant after the tissues have healed sufficiently if it is made of magnesium-based materials. However, most magnesium alloys suffer from a biodegradation rate that is too high, particularly in the early stage [6–8]. Hydrogen bubbles and surface alkalization can also influence tissue growth during the degradation process. Therefore, it is necessary to modify the surface of Mg alloys in order to mitigate degradation in the initial stage to ensure proper tissue healing and growth. Physical vapor deposition (PVD) is one of the effective coating techniques to reduce the corrosion rate of magnesium alloys in aqueous solutions [9–12] and some PVD coatings such as Al_2O_3/Al and ZrO_2/Zr have been suggested for biomedical applications [13,14].

To reduce the influence of the difference in the physical properties between the hard coating and soft substrate, a proper interlayer can improve coating adhesion. For example, adhesion between a diamond-like carbon (DLC) coating and AZ31 magnesium alloy was improved by incorporating a Cr interlayer [15]. However, there have only been scattered reports on the effects of the interlayer on the electrochemical behavior of the coating/substrate system in a common aqueous solution, let alone the physiological environment. For instance, the CrN/Cr interlayer leads to worse protective effects and even deteriorates the performance of the DLC/Mg system in a NaCl solution compared to the AlN/Al interlayer system [15,16]. Owing to the excellent chemical stability and good biocompatibility, aluminum-based oxides and nitrides have been suggested for biomedical applications [13,17]. Al_2O_3 [13] and AlN [10] have been deposited on AZ91 magnesium alloy with Al as the interlayer. However, different from ceramics with good chemical inertness, metals are relatively active in the physiological environment and may lead to leaching of undesirable ions to the human body. Al is also suspected to cause Alzheimer's disease and muscle fiber damage [18–20]. Therefore, it is better to reduce the Al usage and choose an alternative element. Ti and Zr have good biocompatibility and better corrosion resistance in comparison [21,22], but the effects of a Ti interlayer on the corrosion resistance of the coating/substrate system in physiological environment are still not clear. In this study, we used reactive sputtering to produce a protective ceramic coating on AZ31 magnesium alloy and studied the effects of interlayer (Al or Ti) on the performance of the coating/substrate structure in the simulated physiological environment.

---

* Corresponding author. Tel.: +852 34427724; fax: +852 34420542.
  E-mail address: paul.chu@cityu.edu.hk (P.K. Chu).

Five types of simulated biological fluids, 0.9% sodium chloride (NaCl) solution, simulated body fluids (SBF), Hank's solution, Dulbecco's modified eagle medium (DMEM), and phosphate buffering solution (PBS), are commonly used in *in vitro* assessment of biodegradable magnesium alloys. Among them, DMEM is considered the most suitable for the *in vitro* investigation of the biodegradation behavior of magnesium alloys [23]. Liu et al. [24,25] further found that the addition of albumin significantly suppressed the corrosion reaction on Mg alloy in 0.9% NaCl solution and SBF. In this work, in order to simulate the physiological environment more accurately, we selected the complete cell culture media (DMEM with 10% fetal calf serum) as the test solution, and electrochemical impedance spectroscopy and polarization tests were conducted to investigate the electrochemical corrosion behavior.

2. Experimental details

As-cast AZ31 plates (Mg with 3 wt.% Al and 1 wt.% Zn; $10 \times 10 \times 5$ mm^3) were used in this study. The plates were heated at 300 °C for 24 h and quenched in 10 °C pure water in the homogenization treatment. The coating structure is shown in Fig. 1. The top layer is an insulating ceramic film prepared by reactive sputtering and the interlayer is a conductive metallic film fabricated by direct current (DC) sputtering. An ATC ORION sputtering system was used to prepare the ceramic coatings with Al as the target, argon as the sputtering gas, and nitrogen as the reactive gas. The sputtered Al and Ti films served as the interlayers in the comparative experiments. Prior to deposition, the samples were mechanically polished by up to 1 μm diamond paste and ultrasonically washed using pure ethanol. During deposition, the base pressure was about 3×10^{-3} Pa and the sputtering mode was DC. Both heating and bias voltage were not applied in the deposition process and the important parameters are shown in Table 1.

X-ray photoelectron spectroscopy (XPS) with Al K$_\alpha$ irradiation was used to determine the chemical states and elemental depth was used to determine the chemical states and composition after ion
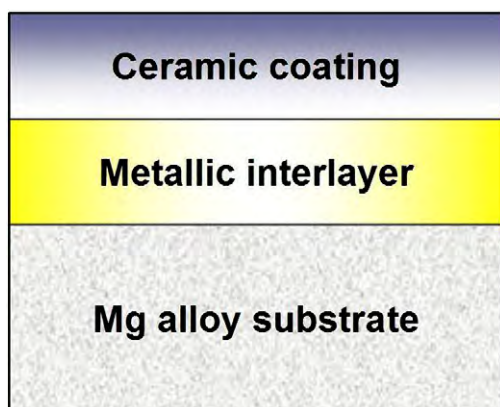

Fig. 1. Schematic representation of the coating/substrate structure.

Table 1
Important processing parameters.

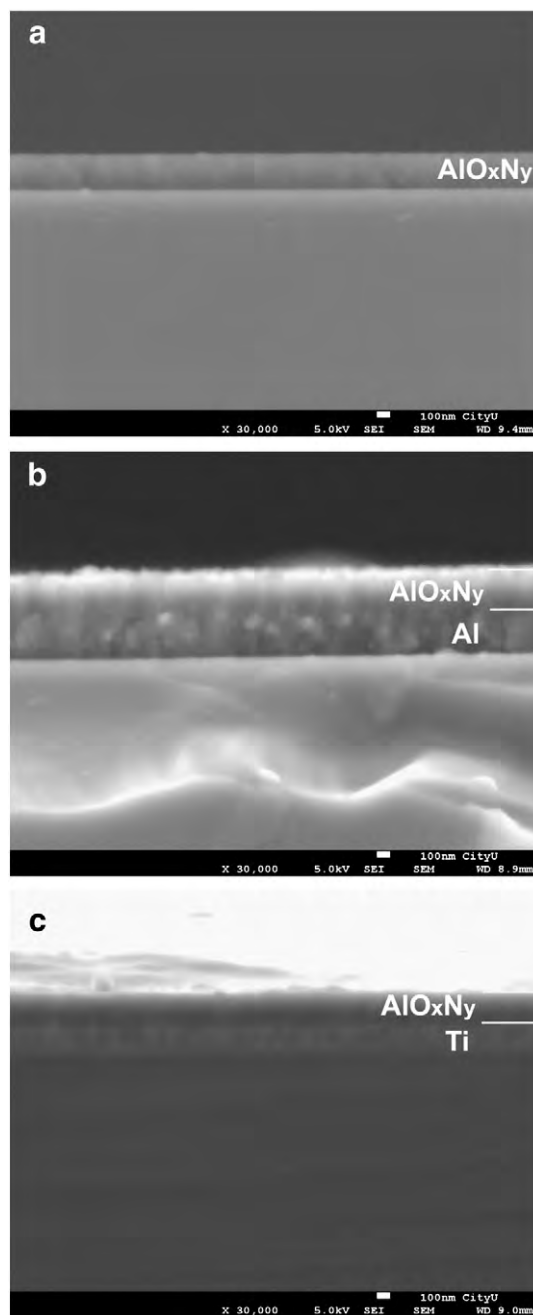| Sample	Layer	Sputtering power (W)	Gas fluence (sccm)		Deposition time (min)
			Ar	N$_2$	
① AlO$_x$N$_y$	AlO$_x$N$_y$	250	20	4	60
② AlO$_x$N$_y$/Al	Al	200	20		30
	AlO$_x$N$_y$	250	20	4	60
③ AlO$_x$N$_y$/Ti	Ti	300	20		30
	AlO$_x$N$_y$	250	20	4	60

Fig. 2. FE-SEM images of the cross-section of the thin films deposited on the silicon substrate: (a) AlO$_x$N$_y$, (b) AlO$_x$N$_y$/Al, and (c) AlO$_x$N$_y$/Ti.

implantation. The sputtering rate was estimated to be about 12 nm min^{-1} based on similar sputtering experiments conducted on a SiO$_2$ reference. The binding energies were referenced to the C 1s line at 285.0 eV. Field-emission scanning electron microscopy (FESEM) was carried out to examine the cross section of the coating structure. Atomic force microscopy (AFM) and scanning electron microscopy (SEM) were employed to study the surface morphology.

A complete cell culture medium consisting of a mixture of Dulbecco's modified eagle medium (Invitrogen Cat no. 11995-040) and 10% fetal calf serum (Hyclone Cat no. SV30087.02) was employed to evaluate the bio-corrosion behavior. The electrochemical experiment was carried out on a Zahner Zennium electrochemical workstation using the conventional three-electrode technique. The potential was referenced to a saturated calomel electrode (SCE) and the counter electrode was a platinum sheet. The specimens with a surface area

of 10×10 mm^2 were exposed to the SBF and the test was carried out at 37 °C. After immersion in the media for 5 min, electrochemical impedance spectra (EIS) were acquired to investigate the electrode/solution interface. The data were recorded from 100 kHz to 100 MHz with a 5 mV sinusoidal perturbing signal at the open-circuit potential. Afterwards, the potential was scanned from the cathodic region to the anodic region at a scanning rate of 1 mV/s in the polarization test. An MTS nano-indenter was used to determine the hardness and elastic modulus in the continuous stiffness measurement (CSM) mode.

3. Results

In this study, FE-SEM is performed to examine the cross-sectional morphology of the coatings and XPS is conducted to analyze the composition of the ceramic layer. XPS reveals the existence of oxygen in the coating possibility as a result of the non-UHV (ultra-high vacuum)

deposition conditions and so the surface coating is technically speaking AlO_xN_y. Fig. 2 shows the cross-section of the coating deposited on Si under the same conditions as described in the Experimental details section above. The flat silicon substrate enables more accurate calculation of the film thicknesses which are basically the same (between 250 and 300 nm) for the Al, Ti, and AlO_xN_y layers. As shown in the high resolution Al_{2p}, N_{1s} and O_{1s} spectra obtained from surface and at depths of 20 nm and 120 nm, the peak shape and position in the spectra obtained from the surface are somewhat different from those in the spectra at greater depths because the surface is contaminated by species from the residual vacuum during deposition or the ambient after deposition. At greater depths, the elemental peak shape and position vary less. The Al_{2p} peak at 74.4 eV, N_{1s} peak at 397.4 eV, and O_{1s} peak at 532.3 eV suggest Al–N and Al–O bonds [26,27]. Fig. 3(d) shows the calculated atomic concentration of each element in the AlO_xN_y coating based on the intensity in Fig. 3(a),
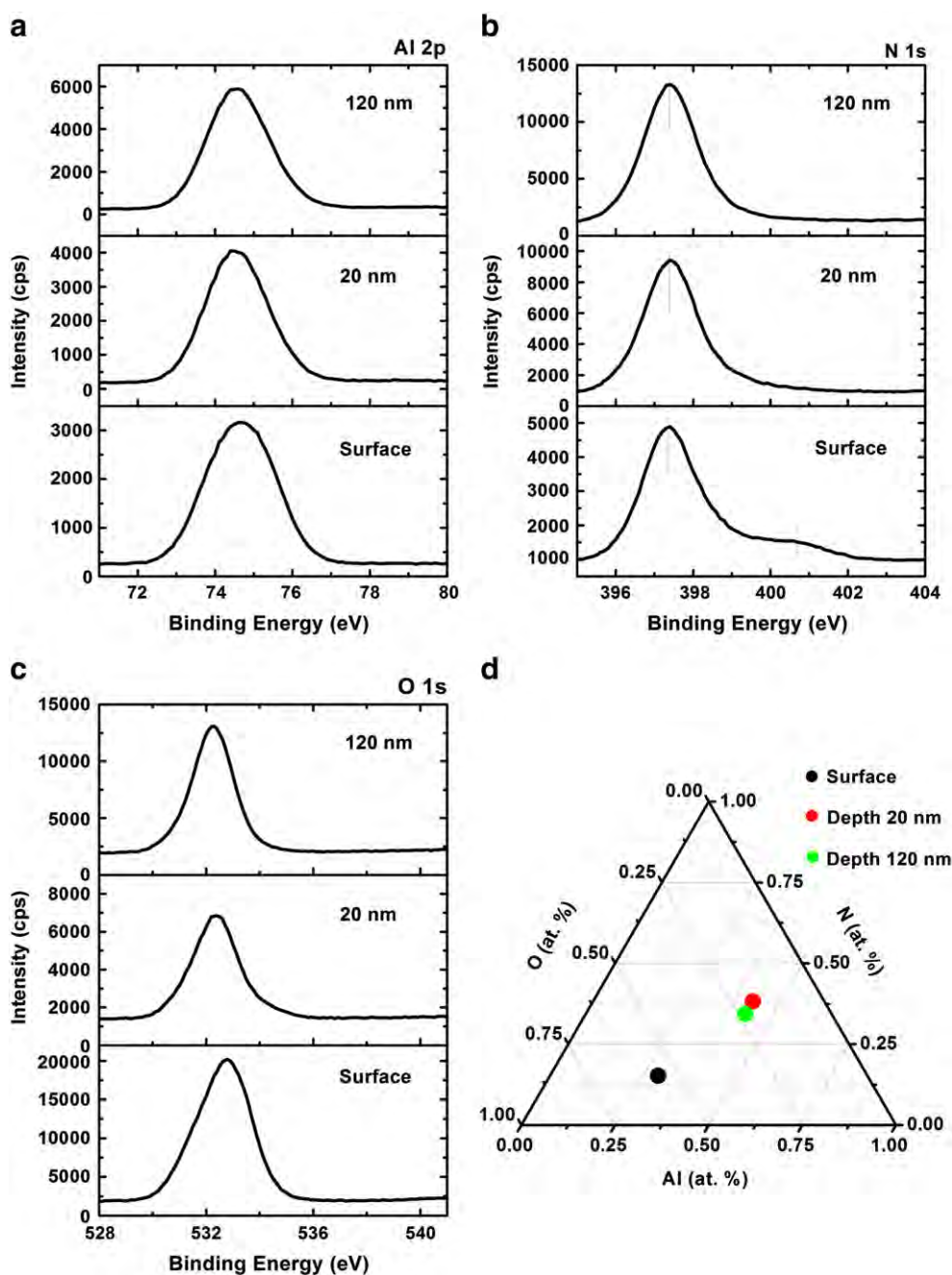

Fig. 3. High resolution XPS spectra of (a) Al 2p, (b) N 1s, and (c) O 1s at different depths. Panel (d) shows the composition at different depths.
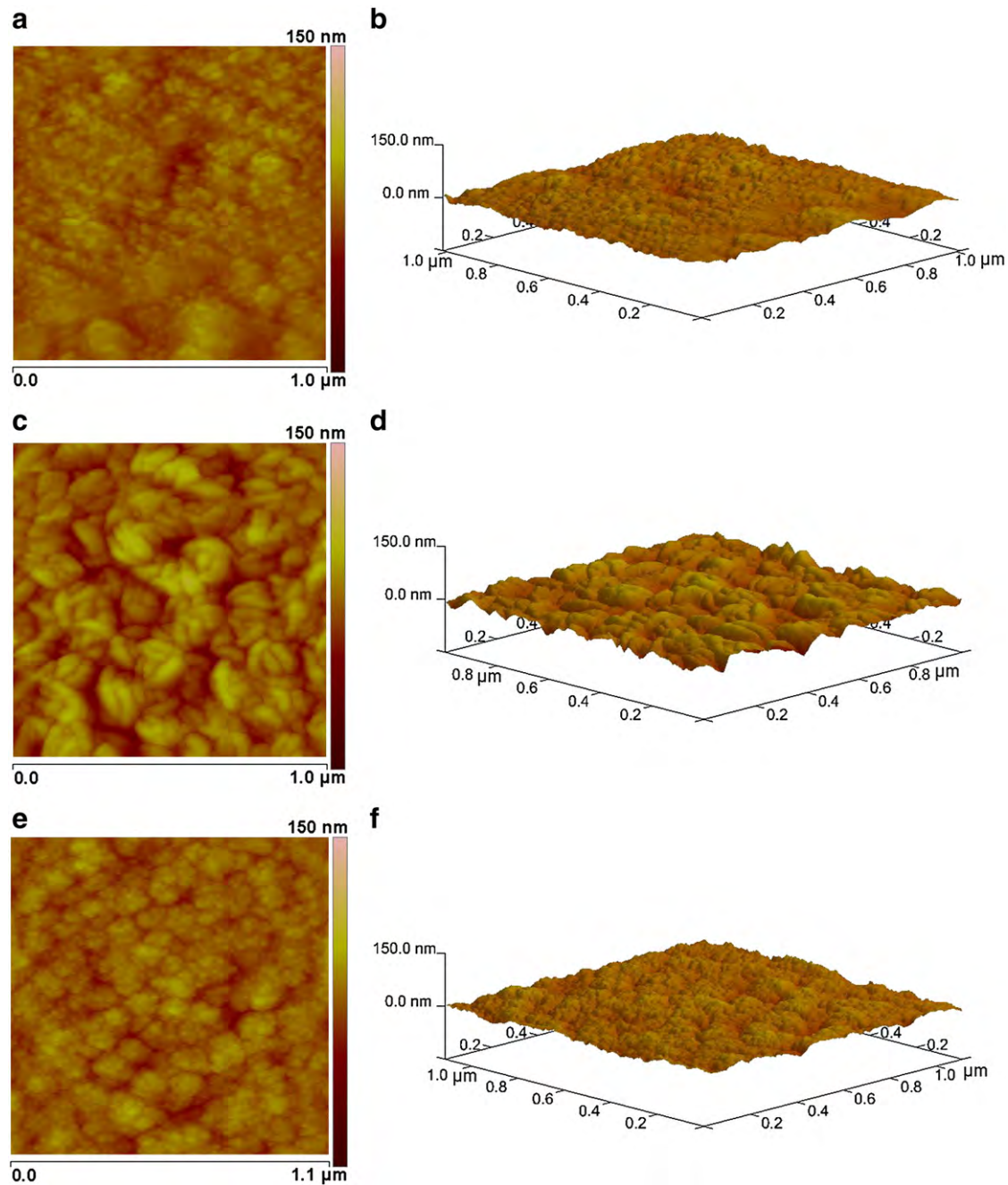
Fig. 4. AFM images of the thin films on Mg alloy substrate: (a) and (b) AlO_xN_y, (c) and (d) AlO_xN_y/Al, (e) and (f) AlO_xN_y/Ti. Panels (a), (c) and (e) show the plan view of surface morphology. Panels (b), (d) and (f) show the 3D view of surface morphology.

(b) and (c) and the atomic concentrations are similar at depths of 20 nm and 120 nm with Al being 42.7%, N 36.3%, and O 21.0%.

Fig. 4 depicts the surface morphology of the coatings at high magnification obtained by AFM and Fig. 5 shows a lower magnification based on SEM. The AFM images indicate that the films are dense on the micro-scale but the SEM picture reveals some random defects several tens of micrometers in size in the three coatings.

Fig. 6(a) and (b) shows the hardness and Young's elastic modulus values of the samples as a function of displacement, respectively. With increasing indentation depths, the hardness decreases gradually finally reaching a stable value corresponding to that of the Mg alloy substrate. The elastic modulus exhibits a similar tendency as hardness. The data suggest that the coatings improve the surface mechanical properties of the magnesium alloy. However, a closer analysis shows that the surface hardness of AlO_xN_y/Al and elastic modulus

are smaller than those of AlO_xN_y/Ti and AlO_xN_y. This may be due to the softer Al interlayer.

Electrochemical impedance spectra (EIS) are acquired to study the electrochemical reaction mechanism at the interface between the metal electrode and simulated biological fluids in the cell culture media. Fig. 7 shows that the capacitive loops of the samples coated with AlO_xN_y/Al and AlO_xN_y are enlarged compared to the bare AZ31 whereas that of the sample coated with AlO_xN_y/Ti is reduced. According to the physical structure of the electrode, an equivalent circuit model with two time constants is outlined in Fig. 7 and used to fit the measured data. Usually on magnesium and magnesium alloys, corrosion is affected by the thin surface oxide film and dissolution typically occurs in the oxide-free areas [28]. Moreover, the corrosion products can cover the surface [4]. Therefore, we simplify the surface characteristics of the AZ31 alloy and use the same model as the
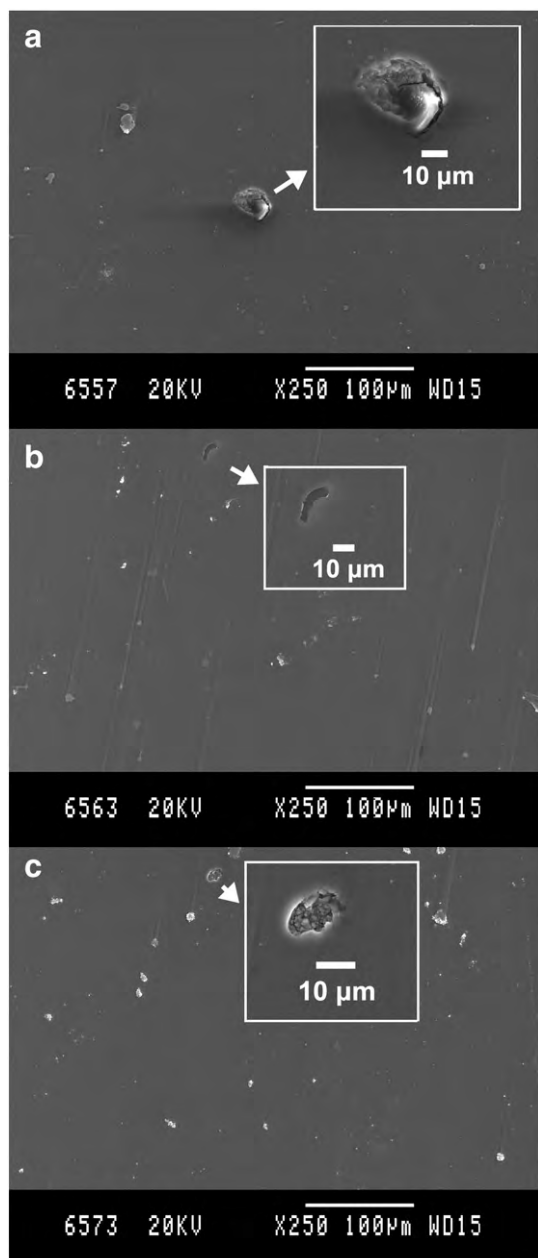
Fig. 5. SEM images of the surface morphology of (a) AlO$_x$N$_y$, (b) AlO$_x$N$_y$/Al, and (c) AlO$_x$N$_y$/Ti on the Mg alloy substrate.

coated alloy. Here, R_s is the solution resistance between the reference electrode and working electrode. A constant phase element CPE_{dl} represents the capacitance of the double layer and R_t is the charge transfer resistance related to the electrochemical reaction. Another constant phase element, CPE_f, denotes the capacitance of the surface film and R_{pore} is the total resistance of the pores in the surface film [29–31].

The experimental data are fitted based on the equivalent model and the fitted values for the individual electrical components are listed in Table 2. Because R_s corresponds to the solution resistance, it is small and similar in all the EIS tests. R_t is related to charge transfer and R_{pore} is associated with the pore resistance of the surface film. Both are critical parameters needed to evaluate the corrosion resistance. In the AlO$_x$N$_y$/Al and AlO$_x$N$_y$ samples, both R_t and R_{pore} are significantly improved compared to the bare AZ31. However, in the AlO$_x$N$_y$/Ti sample, R_t is much smaller. Therefore, the EIS results indicate that the Ti layer reduces the corrosion resistance of the system.
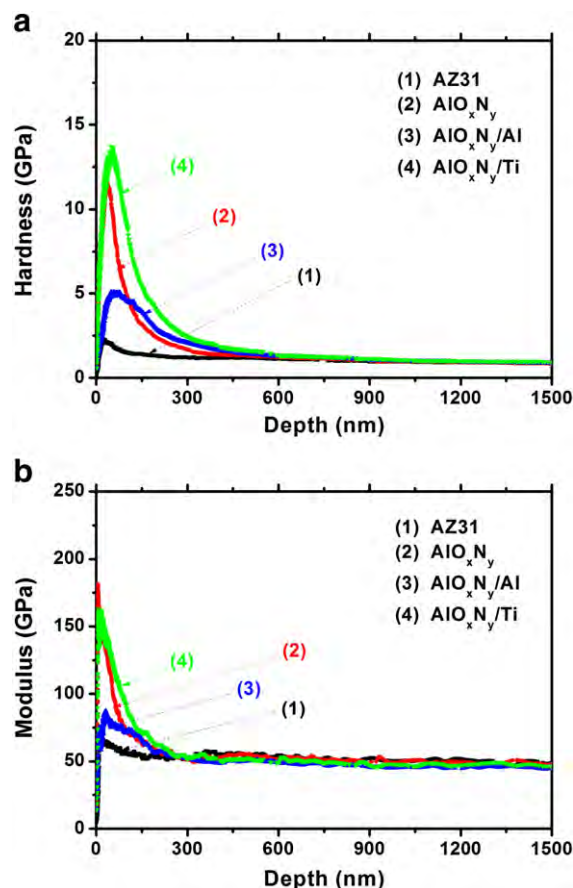

Fig. 6. (a) Hardness and (b) elastic modulus of the samples as a function of displacement.

Fig. 8 shows the polarization curves of the samples in the cell culture media. The cathodic polarization curve represents cathodic hydrogen evolution *via* water reduction and the anodic curve represents dissolution of the sample. The bare AZ31, AlO$_x$N$_y$/Al, and AlO$_x$N$_y$ exhibit a two-regime anodic polarization behavior. The dissolution rate abruptly turns from slow to rapid as the potential is raised in the anodic region. In comparison, AlO$_x$N$_y$/Ti just exhibits a simple activation-controlled anodic behavior. Because the anodic polarization curves do not clearly indicate a Tafel region, the corrosion potential and corrosion current density are derived directly from the cathodic polarization curves and Table 3 gives the corrosion potential and corrosion current densities. After deposition of the AlO$_x$N$_y$ layer,
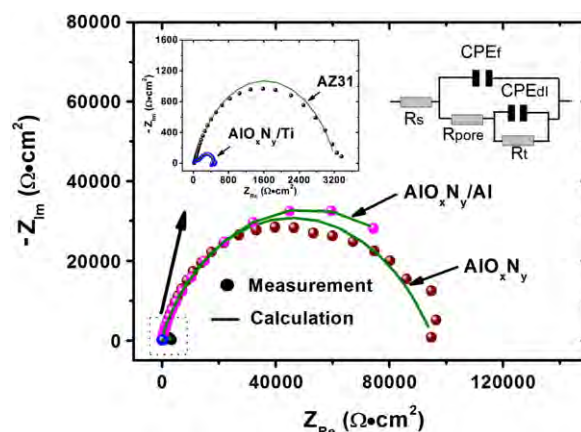

Fig. 7. Electrochemical impedance spectra (EIS) of the samples in the cell culture media. The given equivalent circuit model is used to fit the corresponding curves.

Table 2
Fitted data of the electrochemical impedance spectra in the cell culture media based on the corresponding equivalent circuit model.

Sample	R_s ($\Omega\ cm^2$)	$Y0_f$ ($\Omega^{-2}\ cm^2\ s^{-n}$)	n_f	R_{pore} ($\Omega\ cm^2$)	$Y0_{dl}$ ($\Omega^{-2}\ cm^2\ s^{-n}$)	n_{dl}	R_t ($\Omega\ cm^2$)
AZ31	19.13	2.131×10^{-5}	0.7213	52.95	3.973×10^{-6}	0.8437	3171
AlO_xN_y	12.45	6.855×10^{-8}	0.9363	1196	5.585×10^{-7}	0.6445	9.461×10^4
AlO_xN_y/Al	25.13	3.563×10^{-6}	0.8669	1.589×10^4	5.665×10^{-6}	0.5919	8.992×10^4
AlO_xN_y/Ti	20.8	1.25×10^{-5}	0.5978	137.8	3.968×10^{-5}	0.7569	320.1
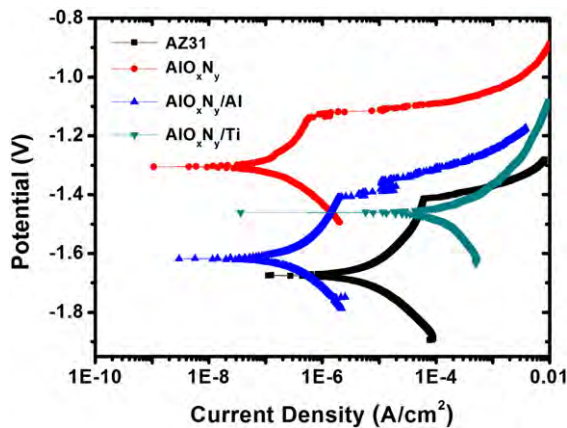
Fig. 8. Polarization curves of the coated and uncoated samples in the cell culture media.

the corrosion current density is significantly reduced and addition of the Al interlayer does not alter the corrosion current density significantly. But, the AlO_xN_y/Ti samples show a larger corrosion current density than bare AZ31, suggesting that the Ti layer reduces the corrosion resistance in the cell culture media similar to the trend revealed by analysis of the EIS results.

4. Discussion

An interlayer is commonly used between a hard ceramic coating and soft substrate to enhance the coating bonding and adhesion, but its effect on other properties, particularly electrochemical corrosion resistance, has received less attention. In coatings deposited by common PVD methods, pores and cracks are common [10,11,16] and accidental scratching possibly leads to a local failure. In this study, the thickness of the AlO_xN_y coating is smaller than that of AlO_xN_y/Al and AlO_xN_y/Ti, but the protective effect is not worse. Addition of a Ti interlayer increases the total thickness but gives rise to more rapid corrosion, implying that the failure stems from coating defects rather than coating thickness. In comparison, although the Al interlayer has a negative effect on the surface mechanical properties of the system, it improves the corrosion resistance in the cell culture media.
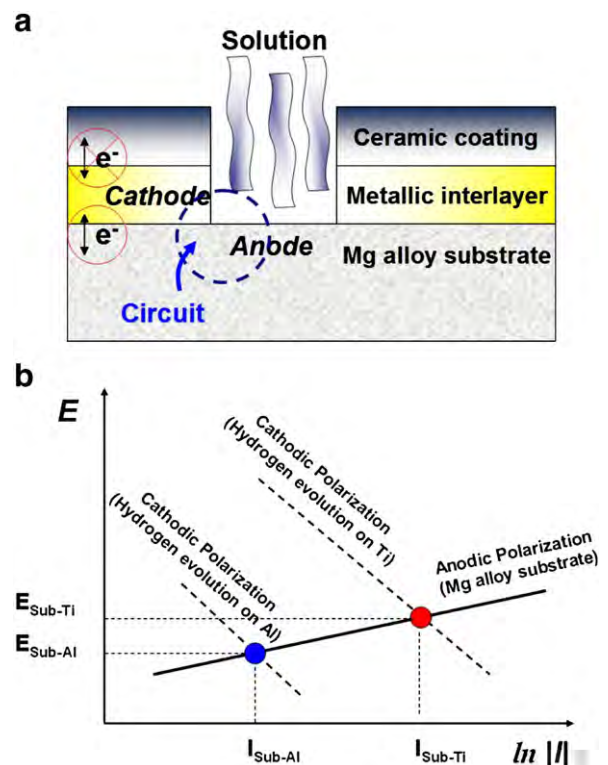
According to the coating defect model proposed by Hoche [32], we postulate a model shown in Fig. 9(a) to explain the corrosion of the coating structure with defects in our study. The aqueous solution first penetrates the defects such as pores, craters, and cracks that

Table 3
Corrosion potential and corrosion current density obtained from the polarization curves.

	Corrosion potential (V)	Corrosion current density (A/cm^2)
AZ31	−1.676	8.868×10^{-6}
AlO_xN_y	−1.303	1.908×10^{-7}
AlO_xN_y/Al	−1.614	3.154×10^{-7}
AlO_xN_y/Ti	−1.460	1.241×10^{-4}

span the entire thickness of the coating and arrives at the interface between the coating and substrate. Because the AlO_xN_y ceramic layer is electrically insulating, it is hard for electrons to traverse between the metallic interlayer and AlO_xN_y ceramic layer. However, at the interface between the metallic interlayer and Mg alloy substrate, there are electrical paths for the electrons. Consequently, a corrosion cell is formed between the interlayer and substrate as soon as the solution arrives at the interface. In this galvanic cell, the metallic interlayer acts as the cathode and the Mg alloy substrate acts as the anode. The galvanic current is usually given as follows [33]:

$$I = \frac{E_{Me} - E_{Sub}}{R_{p(Sub)} + R_{p(Me)} + R_s + R_{Me-Sub}}.$$

Where E_{Me} and E_{Sub} are the corrosion potentials of the cathode and anode, respectively, $R_{p(Sub)}$ is the polarization resistance of the anode, $R_{p(Me)}$ is the polarization resistance of the cathode, R_s is the electrical resistance of the electrolyte, and R_{Me-Sub} is the electrical resistance between the anode and cathode.

The current between the anode and cathode depends on E_{Me}-E_{Sub}, $R_{p(Sub)}$, $R_{p(Me)}$, R_s, and R_{Me-Sub}. R_s depends on the electrolyte conductivity and the system geometry whereas R_{Me-Sub} is related to the conductivity between the metallic interlayer and Mg alloy substrate. In the model shown in Fig. 9(a), two electrodes are connected by the solution and the interface between the layers. If the resistance between

Fig. 9. (a) Model of a galvanic corrosion cell formed in a localized defect and (b) simplified Evans diagram to explain galvanic corrosion.

the two electrodes, such as AlO_xN_y layer and metallic layer, is very large, each part will corrode independently according to the above relationship. With regard to the galvanic couple of Sub-Al and Sub-Ti, R_{Me-Sub} and R_s can be neglected because they are small. It is known that $R_{p(Sub)}$ and $R_{p(Me)}$ depend on the electrochemical reaction kinetics. According to the literature [34,35], we simplify the Evans diagram to show the galvanic corrosion here. Usually, based on the galvanic series in seawater, the corrosion potential from low to high is ranked as follows: Mg alloy<Al<Ti [36,37]. Fig. 8 shows that the corrosion potential of AlO_xN_y/Ti is higher than those of AlO_xN_y/Al and AZ31. Therefore, it can be speculated according to the mixed potential theory that the corrosion potential of Ti is still higher than that of Al in the cell culture media. When two different metals constitute a corrosion cell, hydrogen evolution occurs on the nobler metal. Here, no large difference in the cathodic Tafel slopes among samples can be observed from the polarization curves. Because the anodic current at the interlayer and cathodic current at the substrate are negligibly small, the Evans diagram is further simplified as shown in Fig. 9(b). If the interlayer is changed from Al to Ti, the cathodic polarization curve in the figure shifts to the right. Accordingly, restrained by the shape of the anodic polarization curve of the Mg alloy substrate, the corrosion potential is slightly increased and the corrosion current related to corrosion is evidently increased. In reality, interpretation of the experimental results is more complicated than that described by the above model analysis. According to the EIS analysis, the sum of R_{pore} and R_t indicative of the corrosion resistance increases after the addition of Al layer in the AlO_xN_y coating/Mg alloy system. However, in the subsequent polarization test, the increased corrosion current density indicates that the corrosion resistance decreases in the presence of the Al interlayer. In comparison, both the EIS and polarization results show that the corrosion resistance after inserting the Ti layer decreases obviously. It suggests that the AlO_xN_y/Al system deteriorates with immersion time and gradually shows the galvanic effect. Nonetheless, this effect is much weaker than that observed with the Ti layer. In addition, other factors such as the oxide layer on the polished sample and the fetal calf serum in the solution may influence the corrosion process and lead to some ambiguous results. More research is being conducted in our laboratory to clarify the issue completely and new results will be reported in due course.

Some phenomena reported in past studies can also be understood based on our proposed model and associated mechanism. Al_2O_3/Al and Al_2O_3/Ti have been prepared on the AZ31 magnesium alloy in comparative tests [38], but the addition of Ti deteriorates the corrosion resistance of magnesium alloy in a NaCl solution. The failure mechanism can be explained by our model. Xin et al. have applied Al_2O_3/Al and ZrO_2/Zr on AZ91 magnesium alloy [13,14] and when the immersion time increased from 0.5 h to 18 h, the charge transfer resistance (R_t) of ZrO_2/Zr in SBF decreases from $27 \times 10^3 \, \Omega \, cm^2$ to $2.19 \times 10^3 \, \Omega \, cm^2$ and that of Al_2O_3/Al in SBF diminishes from $74.6 \times 10^3 \, \Omega \, cm^2$ to $3.7 \times 10^3 \, \Omega \, cm^2$. The protection offered by the coatings deteriorates with immersion time, suggesting that coating defects play a critical role in the deterioration. In addition, the different R_t values for different interlayers also indicate the effects of the interlayers on the coating characteristics. According to our investigation, the interlayer plays an important role, in addition to the surface coating.

5. Conclusion

The effect of the interlayer on the corrosion resistance of the ceramic coating/Mg alloy substrate system has been investigated in cell culture media. An AlO_xN_y ceramic coating is deposited on the magnesium alloy by reactive sputtering and Ti and Al films served as the interlayer in the ceramic coating/Mg alloy substrate structure.

The AlO_xN_y ceramic coating can reduce the electrochemical activity of AZ31 in the cell culture media and improve the surface mechanical properties. When an interlayer is used, the Ti interlayer increases corrosion of the Mg alloy due to the presence of defects. The Al interlayer compromises the surface mechanical properties, but does not produce negative effects on the degradation in the cell culture media. Our study provides important data to improve the design of the coating system on biomedical magnesium substrate but more optimization is still needed based on the actual requirements in future applications.

References

[1] E. Zhang, L. Xu, K. Yang, Scripta Mater. 53 (2005) 523.
[2] F. Witte, N. Hort, C. Vogt, S. Cohen, K.U. Kainer, R. Willumeit, F. Feyerabend, Curr. Opin. Solid State Mater. Sci. 12 (2008) 63.
[3] B. Zberg, P.J. Uggowitzer, J.F. Löffler, Nat. Mater. 8 (2009) 887.
[4] Y. Song, D. Shan, R. Chen, F. Zhang, E. Han, Mater. Sci. Eng. C 29 (2009) 1039.
[5] X. Gu, Y. Zheng, Y. Cheng, S. Zhong, T. Xi, Biomaterials 30 (2009) 484.
[6] F. Witte, J. Fischer, J. Nellesen, H. Crostack, V. Kaese, A. Pisch, F. Beckmann, H. Windhagen, Biomaterials 27 (2006) 1013.
[7] G. Song, Corros. Sci. 49 (2007) 1696.
[8] Y. Zong, G. Yuan, X. Zhang, L. Mao, J. Niu, W. Ding, Mater. Sci. Eng. B 177 (2012) 395.
[9] H. Hoche, C. Blawert, E. Broszeit, C. Berger, Surf. Coat. Technol. 193 (2005) 223.
[10] H. Altun, S. Sen, Surf. Coat. Technol. 197 (2005) 193.
[11] G. Wu, X. Wang, K. Ding, Y. Zhou, X. Zeng, Mater. Charact. 60 (2009) 803.
[12] G. Wu, K. Ding, X. Zeng, X. Wang, S. Yao, Scr. Mater. 61 (2009) 269.
[13] Y. Xin, C. Liu, W. Zhang, J. Jiang, G. Tang, X. Tian, P.K. Chu, J. Electrochem. Soc. 155 (5) (2008) C178.
[14] Y. Xin, C. Liu, W. Zhang, K. Huo, G. Tang, X. Tian, P.K. Chu, J. Mater. Res. 23 (2) (2008) 312.
[15] G. Wu, L. Sun, W. Dai, L. Song, A. Wang, Surf. Coat. Technol. 204 (2010) 2193.
[16] G. Wu, W. Dai, H. Zheng, A. Wang, Surf. Coat. Technol. 205 (2010) 2067.
[17] R. Gazia, P. Mandracci, F. Mussano, S. Carossa, Surf. Coat. Technol. 206 (2011) 1109.
[18] M. Shingde, J. Hughes, R. Boadle, J. Wills, R. Pamphlett, Med. J. Aust. 183 (2005) 145.
[19] P.C. Ferreira, K.A. Piai, A.M.M. Takayanagui, S.I. Segura-Munoz, Rev. Lat. Am. Enfermagem 16 (2008) 151.
[20] X. Zhang, G. Yuan, L. Mao, J. Niu, P. Fu, W. Ding, J. Mech. Behav. Biomed. 7 (2012) 77.
[21] Y. Ramaswamy, C. Wu, A.V. Hummel, V. Combes, G. Grau, H. Zreiqat, Biomaterials 29 (2008) 4392.
[22] X. Liu, P.K. Chu, C. Ding, Mater. Sci. Eng. R 47 (2004) 49.
[23] Y. Xin, T. Hu, P.K. Chu, J. Electrochem. Soc. 157 (2010) C238.
[24] C. Liu, Y. Wang, R. Zeng, X. Zhang, W. Huang, P. Chu, Corros. Sci. 52 (2010) 3341.
[25] C. Liu, Y. Xin, X. Tian, P.K. Chu, J. Mater. Res. 22 (2007) 1806.
[26] J.F. Moulder, W.F. Stickle, P.E. Sobol, K.D. Bomben, J. Chastain, Handbook of X-ray photoelectron spectroscopy, Physical Electronics Division, Perkin-Elmer Corporation, Minnesota, USA, 1992.
[27] S. Schoser, G. Brauchle, J. Forget, K. Kohlhof, T. Weber, J. Voigt, B. Rauschenbach, Surf. Coat. Technol. 103–104 (1998) 222.
[28] G. Galicia, N. Pebere, B. Tribollet, V. Vivier, Corros. Sci. 51 (2009) 1789.
[29] C. Liu, Q. Bi, A. Leyland, A. Matthews, Corros. Sci. 45 (2003) 1243.
[30] Y. Zhang, C. Yan, F. Wang, W. Li, Corros. Sci. 47 (2005) 2816.
[31] Q. Meng, J. Li, X. Bian, J. Alloys Compd. 424 (2006) 350.
[32] H. Hoche, C. Rosenkranz, A. Delp, M. Lohrengel, E. Broszeit, C. Berger, Surf. Coat. Technol. 193 (2005) 178.
[33] G. Song, B. Johannesson, S. Hapugoda, D. StJohn, Corros. Sci. 46 (2004) 955.
[34] B. Yu, J. Uan, Scr. Mater. 54 (2006) 1253.
[35] M. Lee, K. Moon, K. Kim, I. Bae, S. Baek, Surf. Coat. Technol. 202 (2008) 5603.
[36] H.P. Hack, D. Taylor, 9th edition, Metals Handbook, 13, ASM Metals, Park, Ohio, USA, 1987.
[37] U.K. Mudali, B. Raj, Corrosion Science and Technology, Alpha Science International Ltd, Oxford, U.K., 2008
[38] G. Wu, X. Zeng, G. Li, S. Yao, X. Wang, Mater. Lett. 60 (2006) 674.